CrossMark

RESEARCH PAPER

Numbering-up Y–Y microfluidic chips for higher-throughput solvent extraction of platinum(IV) chloride

Frederik H. Kriel[1] · Stephen Woollam[2] · Ross J. Gordon[3] · Richard A. Grant[3] · Craig Priest[1]

Abstract The application of microfluidic devices to industrial processing is relatively scarce due to the high volumetric throughputs that are generally required. One approach to increasing throughput is massive parallelisation ('numbering-up' or 'scale-out'), which involves the use of many microfluidic devices working in parallel to multiply the overall throughput. Numbering-up is attractive because it is modular and eliminates traditional 'scale-up' stages on the path towards full-scale processing. However, numbering-up presents other challenges, some of which are addressed here for liquid–liquid extraction using Y–Y chips. The theoretical limits were explored using the extraction of hexachloroplatinate(IV) ions as an industry-relevant system (extraction using a secondary amine). Experimental numbering-up from one channel to five, and then ten, in an extraction module is demonstrated, with extraction performance unchanged with increasing throughput. Calculations suggest that further numbering-up to at least a 1000-channel module could be facilitated by minor modifications to the present circuit.

Keywords Numbering-up · Scale-out · Microfluidic · Platinum · Solvent extraction

✉ Craig Priest
craig.priest@unisa.edu.au

1 Future Industries Institute, University of South Australia, Mawson Lakes, Australia

2 Anglo American's Technical Solutions, Johannesburg, South Africa

3 Johnson Matthey Technology Centre, Sonning Common, Reading, UK

1 Introduction

The use of microfluidics to control small-volume, high-value chemical and biological materials is now very common using so-called lab-on-a-chip devices. The attraction of these miniaturised systems is in their ability to reduce the cost, time, and consumption, while increasing ease-of-use. However, these advantages are equally attractive—or perhaps more so—to higher-throughput applications such as industrial syntheses and separations. The high surface-to-volume ratios encountered in microfluidic chips offer faster phase transfer via diffusion, which is relevant to liquid–liquid extractions (SX) (Brody and Yager 1997; Aota et al. 2007; Kralj et al. 2007). The trade-off for the high surface-to-volume ratios afforded by the microscale environment is the small volumetric throughput. In a typical Y–Y microfluidic SX chip (where two liquid streams meet at a Y-junction flow concurrently where mass transfer or solvent extraction (SX) can happen, and then are split from each other again by a Y-junction), the surface-to-volume ratios may be double that in a traditional (bulk-scale) mixer-settler, resulting in faster extraction (Kolar et al. 2016); however, the volumetric throughput might be less than 1 mL/h for a single extraction channel (Minagawa et al. 2001; Nichols et al. 2011; Kriel et al. 2015). Higher throughputs can only be achieved by using many channels in parallel, which is usually referred to as 'numbering-up' or 'scale-out'. Numbering-up requires no scale-up of the channel dimensions. Instead, many channels work in parallel to achieve the desired volumetric throughput. Numbering-up microfluidic channels has been successful in droplet/bubble production (Al-Rawashdeh et al. 2012a, b; Nisisako et al. 2012; Christian 2013), cell sorting (Warkiani et al. 2015), and biochemical reactions (Thorsen et al. 2002; Melin and Quake 2007). However, numbering-up of

Y–Y SX channels requires a careful consideration of the multiphase flow stability and has not be studied to date, which is the motivation for this paper.

SX is of great industrial importance to chemical processing. Mineral processing is particularly reliant on SX: base metals (e.g., Cu, Ni), precious metals (e.g., Au, Pt, Pd), rare earth elements (e.g., Nd, Dy, Tb), and radioisotopes (e.g. U) are all separated using large-scale SX circuits. Many have considered the advantages of microfluidic SX, with the majority of research directed towards informing conventional processing methods. Extraction of cobalt(II) (Minagawa et al. 2001; Ciceri et al. 2013), iron(II) (Tokeshi et al. 2000), copper(II) (Morita et al. 2010; Priest et al. 2011, 2012), platinum(IV) (Yin et al. 2013; Kriel et al. 2015), palladium(II) (Yin et al. 2013), uranium(IV) (Hellé et al. 2014), and various rare earth elements (Kubota et al. 2003; Maruyama et al. 2004; Nishihama et al. 2006; Hellé et al. 2014) has been demonstrated using microfluidic SX. In every case, throughputs are in the range of mL/h, i.e. many orders of magnitude less than industrial scales. We have focused on industry-relevant extraction conditions including the use of leach solutions derived from acid leaching ores (Priest et al. 2012, 2013) to explore the limits of microfluidic SX for industrial application. Most of our studies to date have focused on small-scale (single extraction channel) experiments. Here, the feasibility of higher-throughput microfluidic SX via numbering-up is investigated for refining platinum from a platinum group metal (PGM) leach solution.

2 Experimental

Aqueous platinum solutions (24 g/L) were prepared by dissolving sodium hexachloroplatinate(IV) (Johnson Matthey) in 0.5 M hydrochloric acid. $[PtCl_6]^{2-}$ was extracted using a secondary amine in Solvesso 150 (ASCC). Microfluidic SXs were carried out using Y–Y microfluidic SX chips (ANFF-SA, Australia), as briefly described below and in further detail elsewhere (Priest et al. 2011, 2012, 2013; Kriel et al. 2015). Two channels merge at a Y-junction to form a single microchannel that is partitioned into two by a guide structure which helps stabilize the co-flowing streams (Sato et al. 2003). The contact length in this channel, L, was 129 mm; this is where the extraction takes place. Phase disengagement occurs at a downstream Y-junction and is typically 98 % complete, based on experiments reported elsewhere (Holzner et al. 2015). At liquid–liquid contact, the channel cross-section is asymmetric to tune the organic/aqueous flow rate ratio, as discussed in the Results and discussion section. The procedure for the etching of asymmetrical channels has been reported previously and, in brief, requires a two-step hydrofluoric acid etch of glass (Hibara et al. 2005; Kriel

et al. 2015). Due to the nature of the wet etching, the width of a channel is approximately double the etch depth plus the mask width (i.e. 10 μm + 2 × etch depth).

Flow was driven by pressure pumps (Mitos P-pump, Dolomite) between 50 and 400 kPa with typical flow rates of between 0.2 and 2 mL/h for a single chip. Flow stability in the microchip was monitored using optical microscopy (Olympus, BH2-UMA). UV–Vis absorption (Ocean Optics QE65000) was used to determine the concentration of $[PtCl_6]^{2-}$ using a 2-mm-path-length quartz cuvette or, to avoid dilution steps, a 'pillar cuvette' with 14.2 μm path length (Holzner et al. 2015, Kriel and Priest 2016). Platinum concentration was determined from absorbance measurements at 259 nm, according to Beer's law.

3 Results and discussion

Numbering-up can be achieved by adding parallel channels in the plane (x–y) of a single chip, stacking chips in the z direction to create a 'module', and operating many modules in parallel. In this paper, we assemble microfluidic extraction chips to create a module containing a 2 × 5 microfluidic SX channel array (a ten-channel module) as a proof-of-concept numbering-up exercise. Later, experiments will be presented for numbering-up of a specific (platinum) extraction; however, the theoretical considerations of designing a numbered-up SX module are discussed first.

3.1 Theory

The Hagen–Poiseuille equation relates the flow rate, Q, of an incompressible and Newtonian fluid in a cylindrical channel (radius r) to the pressure drop, P, along the channel length, L, according to:

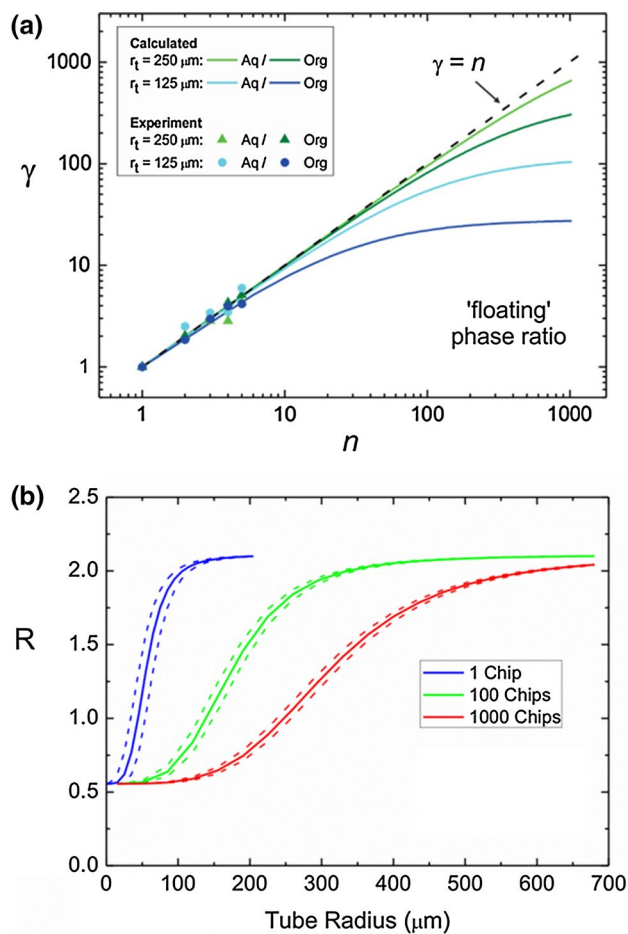$$P = \frac{8\mu L}{\pi r^4} Q \tag{1}$$

where μ is the dynamic viscosity of the liquid. For noncylindrical channels, such as those usually encountered in microfluidic chips, the hydraulic diameter, D, can be used to account for the actual geometry of the channel. For microfluidic SX in a Y–Y chip, the picture is further complicated by the existence of two liquid phases with different viscosities flowing parallel in a single microchannel. We have shown elsewhere that the simple relationship between channel dimensions and phase viscosities, derived from Eq. (1), is useful in designing microfluidic SX channels (Kolar et al. 2016): $R = \frac{\mu_{aq}}{\mu_{org}} \frac{D_{org}^4}{D_{aq}^4}$, where R is the phase ratio of organic to aqueous. For the organic and aqueous phases used in this study, $\frac{\mu_{aq}}{\mu_{org}} = 0.56$. However, numbering-up introduces a more complex fluidic circuit that must
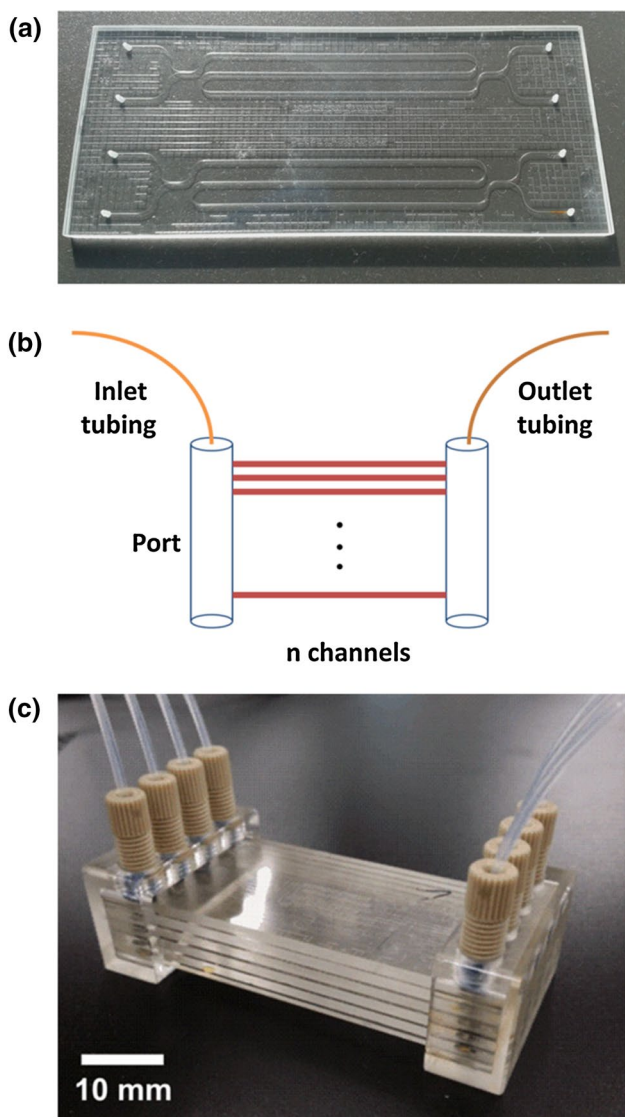
Fig. 1 Illustrations of **a** the chip design and **b** a vertical slice through the port areas of a module setup showing the path of one fluid phase (which is identical for the organic and aqueous phases). **c** an assembled module containing the chip shown in (**a**), i.e. four inlets feed two extraction channels in each chip

Fig. 2 **a** Throughput scaling factor, γ (Eq. (7)), versus number of parallel channels, n, for identical inlet/outlet tubing and ports. The symbols refer to experimental results. **b** The predicted phase ratio, R, for different tube radii. For large tubing radii, the channel dimensions determine R. For small tubing radii, the tubing dimensions determine R

be considered in full to accurately predict the phase ratio under stable flow. Figure 1 shows an illustration of the microfluidic SX chip (containing two extraction channels (Fig. 1a) and module (Fig. 1c)). Each red horizontal line in Fig. 1b represents an individual microchip stacked upon one another such that the inlet/outlet ports (which extend through each chip) are all aligned to create small pressurised chambers (shown as vertical cylinders) that feed a multitude of microchannels with aqueous or organic phase. Figure 1c shows a photograph of an assembled five-chip (ten-channel) microfluidic SX module. The module is fed by four inlets and four outlets (two inlets and two outlets

for each extraction channel). The following derivations consider numbering-up of only one half of this module, i.e. stacking of chips containing only one channel, because the two halves of the module are fed by separate tubing/ports.

The flow path for each phase contains four individual components: inlet tubing, fluid ports, n microchannels, and outlet tubing, as shown in Fig. 1b. The overall pressure drop along this flow path is determined by the sum of the flow resistance of each segment, according to the Hagen–Poiseuille equation. Thus, Eqs. (2), (3), and (4) describe the pressure drop in the segments of tubing, the ports, and the microchannel(s), respectively:

$$P_t = \frac{8\mu L_t}{\pi r_t^4} Q \tag{2}$$

$$P_p = \frac{8\mu L_p}{\pi r_p^4} Q \tag{3}$$

Table 1 Aqueous and organic phase microchannel dimensions

Chip	d_{aq} (μm)	d_{org} (μm)	L_c (mm)
1	37.4	52.8	129
2	39.3	54.5	129
3	38.6	54.2	129
4	39.9	55.3	129
5	39.8	55.0	129

$$P_c = \frac{8\mu L_c}{\pi r_c^4} \frac{1}{n} Q \tag{4}$$

where the subscripts t, p, and c refer to the tubing (inlet and outlet), the fluid ports (inlet and outlet), and the microchannel, respectively, and n is the number of channels in parallel operation. The term $\frac{1}{n}$ in Eq. (4) accounts for the even distribution of total volumetric flow, Q, through the parallel microchannels. In most configurations, the flow resistance in the ports can be ignored, i.e. $P_p \ll P_t + P_c$, and the total pressure drop, ΔP, across the multichannel module is approximated by:

$$\Delta P = \frac{8\mu}{\pi} \left(\frac{L_t}{r_t^4} + \frac{L_c}{r_c^4} \frac{1}{n} \right) Q \tag{5}$$

Assuming the feed pressure is constant for all phases and in all experiments, the relationship between the number of channels operating in parallel and a 'throughput scaling factor', $\gamma = \frac{Q_{n>1}}{Q_{n=1}}$, can be derived:

$$\gamma = \left(\frac{L_t}{r_t^4} + \frac{L_c}{r_c^4} \right) / \left(\frac{L_t}{r_t^4} + \frac{L_c}{r_c^4} \frac{1}{n} \right) \tag{6}$$

or

$$\gamma = \frac{\beta + \alpha}{\beta + \alpha/n} \tag{7}$$

where $\alpha = \frac{L_c}{r_c^4}$ and $\beta = \frac{L_t}{r_t^4}$ are measures of flow resistance in the channel and tubing, respectively.

Equation (7) describes a nonlinear relationship between γ and n. Figure 2a shows the asymptotic dependence for the specific dimensions of the aqueous and organic phase channels (39 and 54 μm etch depths, respectively, and 129 mm length) and tubing (choice of 125 or 250 μm radii and 300 mm length per inlet and outlet tube) used in this study. The feed pressures are set to be equal, as assumed for the derivation of Eq. (7). Note that γ is independent of fluid viscosity and the differences between the organic and aqueous phase curves are due to their respective different channel dimensions and holding the tubing dimensions to be equal. Where the flow resistance in the tubing, β, is negligible compared to that in the channel(s), α, the volumetric flow rate scales proportionally with the number of channels: $\gamma \cong n$. However, as $n \to \infty$, $\alpha/n \to 0$ and γ approaches

an asymptote at $1 + \frac{\alpha}{\beta}$. The result is intuitive: short lengths of large diameter tubing will maximise γ over the greatest range of n. This is shown in Fig. 2 where increasing the inner radius of the tubing from 125 to 250 μm increased the maximum γ by an order of magnitude. Increasing the tubing radius further, e.g. to 500 μm, increases the range of $\gamma \cong n$ over another order of magnitude, i.e. to 1000 channels, representing a 1000-fold increase in volumetric throughput for a microfluidic SX module.

Thus far, the phase ratio, $R = \frac{Q_{org}}{Q_{aq}}$, has not been considered, despite it being a critical parameter in solvent extraction applications. In Y–Y microfluidic SX chips, the dimensions of the aqueous and organic phase channels are varied to tune R. When the organic and aqueous phase inlet/outlet tubing dimensions are chosen to be identical, R is also sensitive to n. In the case that the tubing radii are very large, the pressure drop in the tubing is negligible and R is defined by the channel dimensions ($R \sim 2$). Conversely, when the tubing radii are very small, the pressure drop in the microchannels is negligible and R is defined by the relative viscosity of the two phases ($R \sim 0.56$). The sensitivity of R to n is shown in Fig. 2(b) for $n = 1$, 100, and 1000 channels operating in parallel. The broken lines represent uncertainty in the measurements based on a ± 1 μm error in the geometry of the channels. One can recover the condition $R_{n>1} = R$ by tuning L_t or r_t, regardless of the magnitude of n. For $r_{t(org)} = r_{t(aq)}$, the condition $R_{n>1} = R$ is obtained for $\frac{L_{t(org)}}{L_{t(aq)}} = \frac{r_{c(aq)}^4}{r_{c(org)}^4}$, which is equal to 4.25 for the circuit studied. For $L_{t(org)} = L_{t(aq)}$, the condition $R_{n>1} = R$ is obtained for $\frac{r_{t(org)}}{r_{t(aq)}} = \frac{r_{c(org)}}{r_{c(aq)}}$, which is equal to 1.4 for the circuit studied. Note that tubing length can be varied freely, whereas tubing sizes are generally standardised, meaning that adjusting tubing length to maintain the condition $R_{n>1} = R$ may be more convenient in many cases.
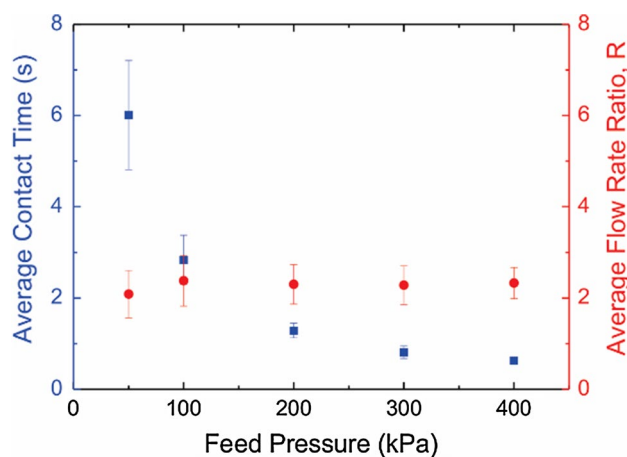
3.2 Numbering-up

We now consider experiments using a numbered-up microfluidic SX module. The five numbered-up chips are shown in Fig. 1. Each chip contains two extraction channels that can be operated independently, i.e. they are parallel and not connected to each other. Thus, experiments can be conducted using one five-channel module or as two parallel modules (ten channels). The chips were designed for a target phase ratio, R, of approximately 2. The channels have a cross-section typical for isotropic etching and characterised by the etch depth, d (Kriel 2014). The average etch depths for the channels containing the aqueous, d_{aq}, and organic, d_{org}, phases were 39 ± 1 μm and 54 ± 1 μm, respectively (Table 1). The inlet ports were chosen to be quite large (0.6 mm diameter) and continue through the entire ~15-mm-thick module of chips, so that the hydrodynamic resistance

(a)

(b)
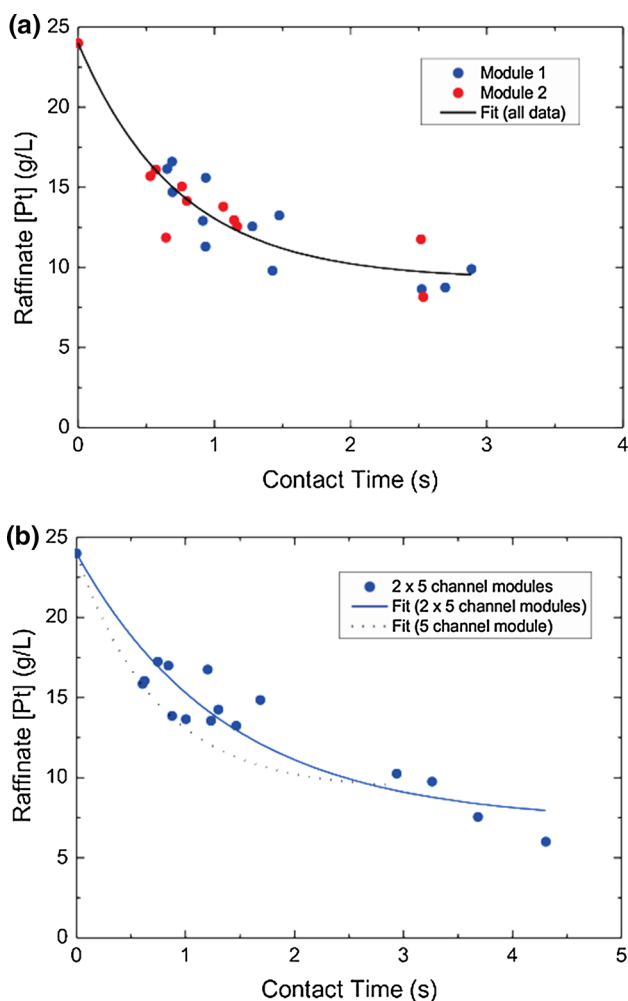
Fig. 3 **a** Results for the two (independent) five-channel modules, identified as Module 1 and Module 2. **b** Results for two five-channel modules in parallel operation, *i.e.* a ten-channel unit. The fits in (**a**) and (**b**), i.e. *solid lines*, assume the first-order kinetics and are forced through 24 g/L Pt at zero contact time. The *broken line* in (**b**) is the best fit for the independent modules and is shown for comparison

Fig. 4 Average contact time and flow rate ratio (organic/aqueous), calculated from all data presented in Fig. 3 and plotted against the feed pressure

along the inlet port is negligible (more than 4 orders of magnitude smaller) compared to that along the microchannel itself, consistent with the assumption in Eq. (7).

Figure 3a shows experimental results for the two (independent) five-channel modules, identified as Module 1 and Module 2 in the figure. The extraction results for the two five-channel modules show some scatter but are in good agreement. The best fit assuming the first-order kinetics is obtained from the combined data set (both modules) and is forced through the initial concentration of 24 g/L Pt. These results demonstrate that numbering-up of microfluidic SX chips can be achieved using a relatively simple module design and that module-to-module differences may be considered negligible. When the two modules are operated together in parallel, i.e. numbering-up of modules, ten channels are being used and the results are shown in Fig. 3b. This experiment gives

the first example of microfluidic SX numbering-up of channels and modules for the Y-Y chip design. Both forms of numbering-up will be essential in approaching the volumetric throughputs required by industry. Fitting the results for the twin-module experiment gave reasonably good agreement with the two single-module experiments, as shown in Fig. 3b.

Although good module-to-module agreement was obtained, the results were more scattered than typically observed for single-chip experiments. This may be attributed to small differences in each channel's dimensions (Table 1) or slight variance in the distribution of flow in individual experiments. Changes in R or contact time can have a significant effect on extraction performance, so we investigated the variation in the experimentally determined R and contact time for different feed pressures, as shown in Fig. 4. We found that the uncertainty in R is largely unchanged for all pressures studied. The uncertainty in the contact time is also small, except for at the lowest feed pressure (50 kPa) where the standard deviation is more than 15 %. Based on this analysis, experimental results for feed pressures of 50 kPa have been omitted in the reported results.

This also illustrates the need to define carefully the operating window for which the feed pressures are sufficiently high, flow is stable, contact time is sufficient, and the length of the channel is not so long that the pressure drop is too large or the stabilising Laplace pressure is breached.

3.3 Industrial feed solution

After dilution with 0.5 M HCl to 24 g/L, a feed solution was extracted using the microSX method at $R \sim 2$ for a single chip, 3-chip module, and 5-chip module (i.e. $n = 1$, 3, and 5, respectively). Figure 5 shows that the results for extraction of Pt from model and feed solutions are very similar for
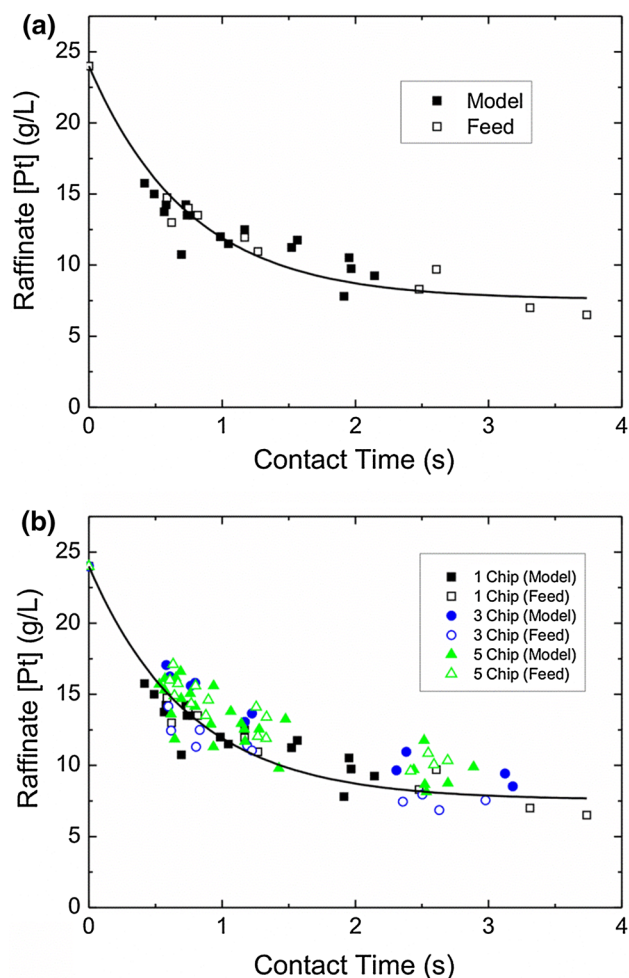
Fig. 5 Concentration of Pt in the raffinate plotted against contact time for feed solution and model Pt solution for **a** single chip (one extraction channel) and **b** single-chip, 3-chip, and 5-chip microSX modules. The *line* represents the best fit the single chip results

each of the modules studied. The significant scatter in the results was observed in both model and feed experiments and can be traced back, at least, in part, to imperfect phase separation. Imperfect phase separation skews the contact time because the flow rates are determined by gravimetric analysis of the collected liquid phases. Nonetheless, there is no difference between the results with model and feed solutions, confirming that numbering-up is not restricted to clean laboratory standard solutions.

4 Conclusion

Several key aspects of Pt microSX were studied for numbering-up, including the extraction rate, flow rate ratio, and number of channels in parallel. Results for multi-chip modules containing up to 5 chips (5 or 10 channels depending on the flow configuration) gave model and feed

extraction results that were in good agreement with those determined for individual channels. Theoretical calculations revealed the sensitivity of the flow rate ratio and scaled flow rate to the channel dimensions, inlet/outlet tubing radii, and number of channels in parallel operation. Limits for the scaled flow rate can be attributed to the relative flow resistance in the tubing and microchip module, and design rules can be established based on theoretical models. The experimental results show good agreement with theoretical predictions over the limited range of n accessible in this study.

References

Al-Rawashdeh M, Fluitsma LJM, Nijhuis TA, Rebrov EV, Hessel V, Schouten JC (2012a) Design criteria for a barrier-based gas–liquid flow distributor for parallel microchannels. Chem Eng J 181–182:549–556

Al-Rawashdeh M, Yu F, Nijhuis TA, Rebrov EV, Hessel V, Schouten JC (2012b) Numbered-up gas–liquid micro/milli channels reactor with modular flow distributor. Chem Eng J 207–208:645–655

Aota A, Nonaka M, Hibara A, Kitamori T (2007) Countercurrent laminar microflow for highly efficient solvent extraction. Angew Chem-Int Ed 46(6):878–880

Brody JP, Yager P (1997) Micromechanics sections of sensors and actuators diffusion-based extraction in a microfabricated device. Sens Actuators, A 58(1):13–18

Christian H (2013) Large-scale droplet production in microfluidic devices—an industrial perspective. J Phys D Appl Phys 46(11):114008

Ciceri D, Mason LR, Harvie DJE, Perera JM, Stevens GW (2013) Modelling of interfacial mass transfer in microfluidic solvent extraction: part II. Heterogeneous transport with chemical reaction. Microfluid Nanofluid 14(1–2):213–224

Hellé G, Mariet C, Cote G (2014) Liquid–liquid microflow patterns and mass transfer of radionuclides in the systems Eu(III)/HNO/DMDBTDMA and U(VI)/HCl/Aliquat 336. Microfluid Nanofluid 17(6):1113–1128

Hibara A, Iwayama S, Matsuoka S, Ueno M, Kikutani Y, Tokeshi M, Kitamori T (2005) Surface modification method of microchannels for gas–liquid two-phase flow in microchips. Anal Chem 77(3):943–947

Holzner G, Kriel FH, Priest C (2015) Pillar cuvettes: capillary-filled, microliter quartz cuvettes with microscale path lengths for optical spectroscopy. Anal Chem 87(9):4757–4764

Kolar E, Catthoor RPR, Kriel FH, Sedev R, Middlemas S, Klier E, Hatch G, Priest C (2016) Microfluidic solvent extraction of rare earth elements from a mixed oxide concentrate leach solution using Cyanex® 572. Chem Eng Sci 148:212–218

Kralj JG, Sahoo HR, Jensen KF (2007) Integrated continuous microfluidic liquid–liquid extraction. Lab Chip 7(2):256–263

Kriel FH, Priest C (2016) Influence of sample volume and solvent evaporation on absorbance spectroscopy in a microfluidic "pillar-cuvette". Anal Sci 32(1):103–108

Kriel FH, Priest C, Ralston J, Parkinson L, Woollam S, Plint N, Grant RA, Ash P (2014). Extraction and throughput for micro-solvent extraction of platinum using a single chip and a multi-chip module. International solvent extraction conference. Würzburg, Germany

Kriel FH, Holzner G, Grant RA, Woollam S, Ralston J, Priest C (2015) Microfluidic solvent extraction, stripping, and phase disengagement for high-value platinum chloride solutions. Chem Eng Sci 138:827–833

Kubota F, Uchida JI, Goto M (2003) Extraction and separation of rare earth metals by a microreactor. Solv Extr Res Dev-Jpn 10:93–102

Maruyama T, Matsushita H, Uchida J, Kubota F, Kamiya N, Goto M (2004) Liquid membrane operations in a microfluidic device for selective separation of metal ions. Anal Chem 76(15):4495–4500

Melin J, Quake SR (2007) Microfluidic large-scale integration: the evolution of design rules for biological automation. Annu Rev Biophys Biomol Struct 36(1):213–231

Minagawa T, Tokeshi M, Kitamori T (2001) Integration of a wet analysis system on a glass chip: determination of Co(II) as 2-nitroso-1-naphthol chelates by solvent extraction and thermal lens microscopy. Lab Chip 1(1):72–75

Morita K, Hagiwara T, Hirayama N, Imura H (2010) Extraction of Cu(II) with dioctyldithiocarbamate and a kinetic study of the extraction using a two-phase microflow system. Solv Extr Res Dev-Jpn 17:209–214

Nichols KP, Pompano RR, Li L, Gelis AV, Ismagilov RF (2011) Toward mechanistic understanding of nuclear reprocessing chemistries by quantifying lanthanide solvent extraction kinetics via microfluidics with constant interfacial area and rapid mixing. J Am Chem Soc 133(39):15721–15729

Nishihama S, Tajiri Y, Yoshizuka K (2006) Separation of lanthanides using micro solvent extraction system. Ars Sep Acta 4:18–26

Nisisako T, Ando T, Hatsuzawa T (2012) High-throughput production of single and compound emulsions via on-chip microfluidic parallelization coupled with coaxial multiple annular world-to-chip interfaces. 16th international conference on miniaturized systems for chemistry and life sciences Okinawa, Japan, Royal Society of Chemistry, pp 914–917

Priest C, Zhou J, Sedev R, Ralston J, Aota A, Mawatari K, Kitamori T (2011) Microfluidic extraction of copper from particle-laden solutions. Int J Miner Process 98(3–4):168–173

Priest C, Zhou J, Klink S, Sedev R, Ralston J (2012) Microfluidic solvent extraction of metal ions and complexes from leach solutions containing nanoparticles. Chem Eng Technol 35(7):1312–1319

Priest C, Hashmi SF, Zhou J, Sedev R, Ralston J (2013) Microfluidic solvent extraction of metal ions from industrial grade leach solutions: extraction performance and channel aging. J Flow Chem 3(3):76–80

Sato K, Hibara A, Tokeshi M, Hisamoto H, Kitamori T (2003) Microchip-based chemical and biochemical analysis systems. Adv Drug Deliv Rev 55(3):379–391

Thorsen T, Maerkl SJ, Quake SR (2002) Microfluidic large-scale integration. Science 298(5593):580–584

Tokeshi M, Minagawa T, Kitamori T (2000) Integration of a microextraction system on a glass chip: ion-pair solvent extraction of Fe(II) with 4,7-diphenyl-1,10-phenanthrolinedisulfonic acid and tri-n-octylmethylammonium chloride. Anal Chem 72(7):1711–1714

Warkiani ME, Wu L, Tay AKP, Han J (2015) Large-volume microfluidic cell sorting for biomedical applications. Annu Rev Biomed Eng 17(1):1–34

Yin C-Y, Nikoloski AN, Wang M (2013) Microfluidic solvent extraction of platinum and palladium from a chloride leach solution using Alamine 336. Miner Eng 45:18–21